An Experimental Study of the Dynamic Behavior of Stick-Slip on a Nonuniform Strength Fault

An Experimental Study of the Dynamic Behavior of Stick-Slip on a Nonuniform Strength Fault

NAOYUKI KATO*, YASUTO KUWAHARA**, KIYOHIKO YAMAMOTO*,
and TOMOWO HIRASAWA*

(Received December 26, 1988)

Abstract: Laboratory experiments were carried out for clarifying the effect of nonuniform strength distribution of sliding surfaces upon the dynamic behavior of shear instability. Stick-slip events were generated on a pre-existing fault in a granite sample. The sliding surfaces were artificially undulated so as to produce a nonuniform distribution of normal stress or shear strength on the fault, where highly pressed regions of the fault can be regarded as asperities. The asperities were found to have a significant effect on the initiation and the termination of rupture. A rupture developed in a weak region sometimes stops propagating at an asperity. When the asperity is broken, the complete slip that would extend over the entire fault starts propagating. We determined the local values of the breakdown stress drop $\Delta\tau_b$, the maximum slip velocity $\dot{u}_{max}$, the rupture velocity V_R, and the normal stress σ_n. It is found that the values of $\Delta\tau_b$, $\dot{u}_{max}$, and σ_n are large in the asperities while the value of V_R is small. The nonuniformities in spatial distributions of these values are all decreased with an increase in the normal stress applied to the fault. The decrease rate in nonuniformity of the shear strength of the fault is singnificantly lower than that of the local normal stress on the fault. Roughly speaking, the observed values of $\Delta\tau_b/\sigma_n$ and $(\dot{u}_{max}/V_R) \cdot (\mu/\Delta\tau_b)$ are found to be nearly constant, where μ is the rigidity. Rigorously speaking, however, they are not constant; $\Delta\tau_b/\sigma_n$ depends upon the rupture velocity and the value of $(\dot{u}_{max}/V_R) \cdot (\mu/\Delta\tau_b)$ at a point is affected by the strength distribution in the surrounding area on the fault.

1. Introduction

Brace and Byerlee (1966) have suggested that stick-slip events on a pre-existing fault in rock are considered to have the mechanism similar to that of crustal earthquakes. Since then numerous stick-slip experiments have been made to obtain a general understanding for the physical process of earthquake occurrence.

Experimental studies have revealed so far some characteristics of the dynamic process of shear rupture propagation. Johnson *et al.* (1973) and Johnson and Scholz (1976) studied the source parameters of rupture volocity, slip velocity, and stress drop for the stick-slip events observed in their laboratory experiments using rock samples. Their values of the rupture velocity are nearly equal to S-wave velocity of the rock sample, and this is consistent with the results estimated for natural earthquakes. They found a linear relation between the stress drop and the slip velocity as predicted theoretically by Brune (1970) and by Sato and Hirasawa (1973). Similar results have been

---
* Observation Center for Prediction of Earthquakes and Volcanic Eruptions, Faculty of Science, Tôhoku University, Sendai 980
** Geological Survey of Japan, Tsukuba 305

reported in the stick–slip experiments on the sample made of CR–39 plastic material by Wu *et al.* (1972) and on the samples made of foam rubber material by Brune (1973) and by Archuleta and Brune (1975).

Many recent experimental data of stick–slip have been analyzed in terms of the slip-weakening model introduced by Ida (1972) and by Palmer and Rice (1973). Okubo and Dieterich (1981, 1984) observed for stick–slip events the breakdown process similar to that in the model. They estimated the apparent fracture energy and found its dependences on the normal stress and on the fault roughness. Kuwahara (1985) examined in detail the effect of fault roughness on the dynamic property of shear faulting. He quantitatively characterized the roughness of sliding surfaces by the cut–off wavelength λ_c in the power spectrum of the fault roughness, and proposed a scaling law for shear instability by taking λ_c as a scaling parameter. An extensive study of stick–slip experiment has been made by Ohnaka *et al.* (1986). According to them, the breakdown zone that expands slowly in the nucleation process contracts its size rapidly when the crack tip begins propagating dynamically. They further discussed the mechanism of irregular faulting and suggested that the radiation of high frequency waves was enhanced by the irregularity of sliding surface waviness.

The source process of an earthquake like a multiple shock is an important issue in seismology, since the high frequency wave radiation from such an earthquake often gives rise to great property damage. The irregular faulting of an earthquake should be caused by some nonuniform distributions of stress and/or strength on faults. The region of a high strength on a fault may be expected to be a stress concentrator like an asperity on one hand and to be a stress barrier on the other hand. This implies that the nonuniformity of fault surfaces should affect both the initiation and the termination process of earthquake faulting. It must be very important, therefore, not only for the engineering seismology but also for the earthquake prediction to elucidate the effect of the nonuniformity upon the faulting process.

The theoretical studies using numerical simulation methods have been made on the effect of nonuniform distributions of stresses or strength by, for instance, Das and Aki (1977), Mikumo and Miyatake (1978), and Israel and Nur (1979). These stuides have made a considerable contribution to promoting our physical understanding of the complex behavior of earthquake faulting. The most important, however, seems to be to find experimentally the constitutive law valid for the breakdown process in the rupture front region of earthquake faulting. In spite of its importance, there are few systematic laboratory experiments on the problem due probably to difficulties in artificially forming the surface nonuniformities of simulated faults with a limited length.

We will examine in the present study the effect of nonuniform stress or strength distribution of sliding surfaces upon the dynamic behavior of shear instability on a 40 cm long simulated fault in a granite sample. The artificially introduced waviness of the sliding surfaces are expected to result in a nonuniform stress field on the fault. Shear strains along the fault and relative displacements across the fault are recorded as functions of time. Since the wavelength of the surface waviness is designed to be much

longer than the mutual distance of two neighboring sensors along the fault, it is possible to observe the details of the breakdown process of the asperity, which is defined by a relatively strong region on a fault. The main purpose of the present paper is to examine in detail the relationships among the physical parameters describing the dynamic behavior of stick-slip such as breakdown stress drop, slip velocity, rupture velocity, and local normal stress.

2. Experimental Procedure

A rock sample was biaxially pressed at a constant strain rate with a loading apparatus to generate stick-slip events on a simulated fault. The sample of Higashiyama granite of 30 cm×30 cm×10 cm in size has a diagonally pre-cut fault of about 40 cm in length (Fig. 1). The P and S wave velocities of the sample are 5.5 km/s and 3.3 km/s, respectively. The Young's modulus, rigidity, and Poisson's ratio, which should be regarded as static and effective elastic constants, are 5.6×10^4 MPa, 2.4×10^4 MPa, and 0.17, respectively. The sliding surfaces of the granite blocks were carefully prepared as will be described in the next section.

The biaxial loading apparatus is capable of pressing a large sample of 30 cm×30 cm×30 cm with the maximum loads of 2.9×10^6 N in the x-axis and 4.9×10^6 N in the y-axis. The loads in the two directions can independently be controlled by the respective servo-mechanisms. Fig. 2 shows an example of the time histories of average shear and average normal stresses applied to the simulated fault to generate a stick-slip event. They were calculated from the output signals of pressure transducers for the rams in the two axes. Referring to the numbers given in Fig. 2, our loading operation is explained as follows: 1) The average normal stress was adjusted to a prescribed value by the manual operation for the ram pressures. This operation was necessary because an offset in the average normal stress had been caused by the occurrence of the preceding stick-slip event. 2) The ram displacement in the x-axis was increased at a constant strain rate and the ram pressure in the y-axis was decreased at a constant rate through
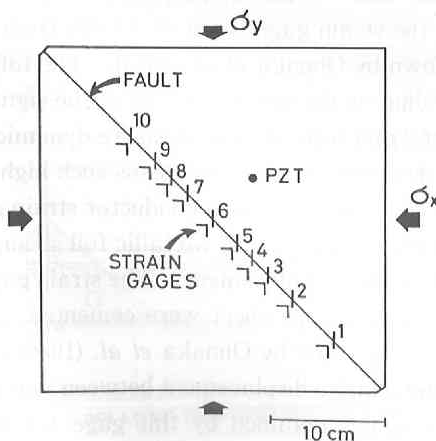

Fig. 1 Schematic diagram of rock sample. The channel numbers are indicated for the sensors used.
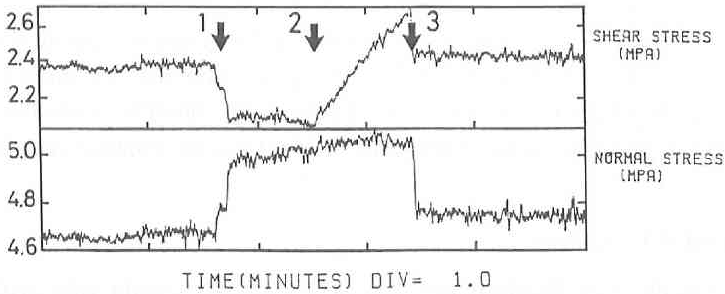
TIME(MINUTES) DIV= 1.0

Fig. 2   The time histories of average shear stress and average normal stress applied
to the simulated fault to show our loading operation for obtaining stick-slip
events successively.
The artificial and natural events are identified as follows ;
1)   loading adjustment for the average normal stress,
2)   the beginning of loading at a constant strain rate, and
3)   the occurrence of a stick-slip event.

respective programmable time functions.   The two time functions for two rams were so
programmed that the average shear strain might be increased at a constant rate while
the average normal stress might be kept constant.   The strain rate was fixed at 10^{-6}/s
throughout our experiment.   3) A stick-slip event occurred and, at the same time, the
average shear stress decreased.   Instantaneously, the pressure in the y-axis increased
and that in the x-axis decreased because of the rapid slip motion between the two blocks
of the rock sample.   Since it is much faster than the response of servo-mechanism, the
average normal stress applied to the fault is expected to stay constant during the stick-
slip motion.   When the servo-mechanism caught the slip motion up after a while, the
ram pressure in the y-axis decreased to decrease the average normal stress.

In order to obtain properly the time functions of relative displacement across the
fault and of stresses near the fault, we used different types of strain gages as sensors.
The frequency response of a strain gage can be determined simply from the relation
between the gage length and the wavelength of the signal concerned, since the frequency
response of gage material itself is sufficiently flat.   When the propagation speed of the
signal is 3 km/s, the frequency response of the strain gage is flat (0–1.8 dB) from DC to
520 kHz for the gage length of 2 mm, as shown by Ohnaka et al. (1983).   The following
three kinds of strain gages were used depending on the characteristics of the signals : 1)
Semiconductor strain gages with a length of 2 mm were used to measure dynamic shear
strains near the simulated fault, where the dynamic shear strain means such high-speed
phenomena as those corresponding to stick-slip events.   A semiconductor strain gage is
about fifty times as sensitive as a metallic foil strain gage.   2) Metallic foil strain gages
with a length of 2 mm were used to measure relative displacement.   The strain gage was
pasted across the fault.   Only the two ends of the gage sheet were cemented, and the
gage part of the sheet was not cemented as illustrated by Ohnaka et al. (1986) in their
Fig. 3.   This makes it possible to measure the relative displacement between two blocks.
Rigorously speaking, however, the strain changes obtained by this gage for relative

displacement should include some contribution from a change in elastic strain of the rock body. The typical value of relative displacement for a stick-slip event is about $10\,\mu$m to give a strain change of 4×10^{-3} strain. This is much larger than the typical value, say, 10^{-5} strain, of shear strain drop in a stick-slip event. Thus, our relative displacement measurement is considered reasonably accurate. 3) Metallic strain gages of a length of 5 mm were used to measure static strains near the fault, where the static strains mean very low-speed phenomena of strain changes. We measured longitudinal strains in three different directions at a 45° interval at a point to determine the shear and normal stresses to the fault plane. All the sensors were aligned at a distance of 5 mm from the fault.

The signals of dynamic shear strain and relative displacement were amplified and high-cut filtered with a cut-off frequency of 500 kHz. Twenty channels of wavememory were employed to record the signals, in which the resolution is 10 bits or 8 bits and the record length is 2048 words. The sampling frequency was either 2 MHz or 1 MHz, according to the frequency characteristics of the signals. This recording system was triggered by an acoustic emission event, which was detected by a piezoelectric transducer and expected to accompany a stick-slip event. The static strain signals were A/D converted and stored in a computer, where the resolution and the sampling frequency were 12 bits and about 6 Hz, respectively.

3. Design of Nonuniform Fault Surfaces

Strength and stress nonuniformities on a fault are considered as the cause of irregular motion in faulting. The macroscopic strength of faults was often described by the apparent fracture energy. Ida (1972) and Palmer and Rice (1973) have proposed the fracture energy criterion for shear fracture propagation based on the slip-weakening model. Fig. 3 schematically illustrates the model with the relation between the relative displacement and the shear stress at a point on the fault surface. The local shear stress, whose initial value is τ_i, increases as a crack tip approaches to the point. When the shear stress reaches its peak value τ_p, a breakdown process begins. That is, the shear stress decreases with ongoing slip, until it reaches the dynamic frictional stress τ_f and, at the same time, the total slip at the point amounts to d_c. The critical displacement is defined by this value of d_c. After that, the slip amount increases further while the shear stress stays at the constant value of τ_f. The shaded area in Fig. 3 expresses the
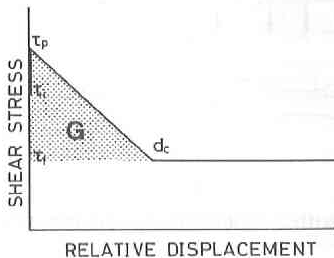

Fig. 3 A schematic representation of the slip-weakening model. The abscissa and the ordinate are the relative displacement and the shear stress at a point on the fault. The τ_i, τ_p, and τ_f stand for initial stress, peak stress, and dynamic frictional stress, respectively. The critical displacement is denoted by d_c. The shaded area represents the apparent fracture energy G.

apparent shear fracture energy G, which is the energy per unit area required for an advance of cracking. The apparent fracture energy G can be approximated by

$$\left.\begin{aligned} G &= (1/2)\, \Delta\tau_b \cdot d_c, \\ \Delta\tau_b &= \tau_p - \tau_f, \end{aligned}\right\} \tag{1}$$

where $\Delta\tau_b$ is called breakdown stress drop.

The normal-stress dependence of the shear fracture energy has been reported in the experimental studies by Okubo and Dieterich (1981, 1984), where the normal stress defined by them should be regarded as the one averaged over the entire fault. We may expect the dependence of the local shear fracture energy on the local normal stress in the present case of the nonuniform fault. In other words, we may expect that a nonuniform strength distribution can be introduced through the nonuniform distribution of local normal stresses. Further, the nonuniform distribution of local normal stresses can artificially be controlled by the waviness of sliding surfaces.

We polished the fault surfaces so carefully that their shape might have a sinusoid-like waviness whose wavelength and amplitude were approximately 10 cm and 5 μm, respectively. Fig. 4 shows the profiles of two mating sliding surfaces measured with a profilometer. We obtained three more profiles measured along three different lines which are parallel to one another on a fault surface. Although the profiles are not shown in the figure, we confirmed that the surface topography did not vary significantly in the direction of the fault width. The two sliding surfaces are nearly symmetric, as seen in the figure. The convex areas of the waviness are expected to be strongly stressed, while the concave areas are weakly stressed. A nonuniform distribution of normal stress on the fault was thus introduced by this pattern of waviness.

The apparent fracture energy depends also on the roughness of sliding surfaces as reported by Okubo and Dieterich (1984) and by Kuwahara (1985). The roughness of a sliding surface is characterized by the cut-off wavelength, λ_c, defined in the power spectrum of the surface topography, as found by Kuwahara (1985). He showed that the λ_c can be controlled by the grit size of abrasive. Since we polished the overall sliding surfaces with the same grit size, we can ignore the effect of nonuniformity of the roughness upon the fracture energy. The value of λ_c is 10 μm for our sliding surfaces.

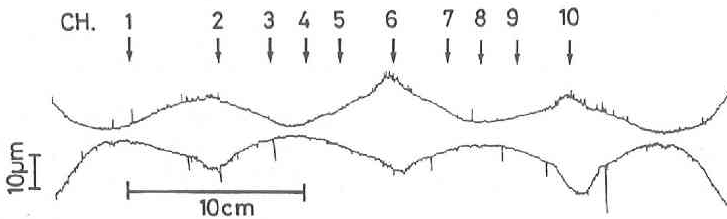Kuwahara *et al.* (1986) have experimentally shown that a shear crack starts to

Fig. 4 Profiles of two sliding surfaces measured with a profilometer. Arrows indicate positions of sensors.

propagate dynamically when the crack length reaches a critical length. They found that the critical crack length L_c, which is defined as the crack length beyond which the rupture velocity exceeds 1/10 of the S–wave velocity, depends on the roughness of sliding surfaces. Their empirical relation is

$$L_c \sim 5000 \; \lambda_c. \tag{2}$$

The predicted value of L_c is 5 cm in our case and shorter than the wavelength of the waviness of 10 cm. This may enable us to observe some special cases of rupture arrest at the convex areas.

4. Experimental Results

4.1 General Observation

A number of stick–slip events were generated on the wavy fault surfaces. Figs. 5 and 6 show examples of the obtained time histories of shear stress, relative displacement, and slip velocity at average normal stresses of 2.5 and 7.5 MPa, respectively. Shear stress records were obtained by multiplying shear strain signals by the rigidity of the rock sample. Being high–cut filtered with a cut–off frequency of 50 kHz, the relative displacement was numerically differentiated with respect to time to give the slip velocity function. The positions of sensors have already been shown in Fig. 4. Sensors for shear strain and for relative displacement were placed not exactly on the same position. The two kinds of sensors were put at a distance ranging from 5 mm to 10 mm.

We determined the rupture velocity V_R, the breakdown stress drop $\Delta\tau_b$, and the maximum slip velocity $\dot{u}_{max}$ at several points along the fault. The velocity V_R was evaluated from the travel time of the rupture front over a distance between two neighboring sensors. The obtained V_R should be regarded as an averaged rupture velocity between the two points of sensors. We took the onset time of sudden slip (relative displacement) as the rupture time. They are indicated by solid triangles in
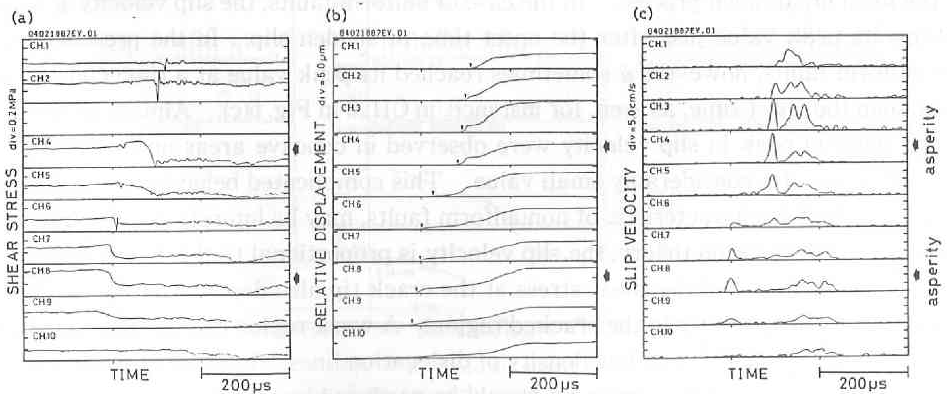

Fig. 5 The observed records of (a) shear stress, (b) relative displacement, and (c) slip velocity for a stick–slip event at an average normal stress of 2.5 MPa. The onset times of rupture are indicated by solid triangles in (b).
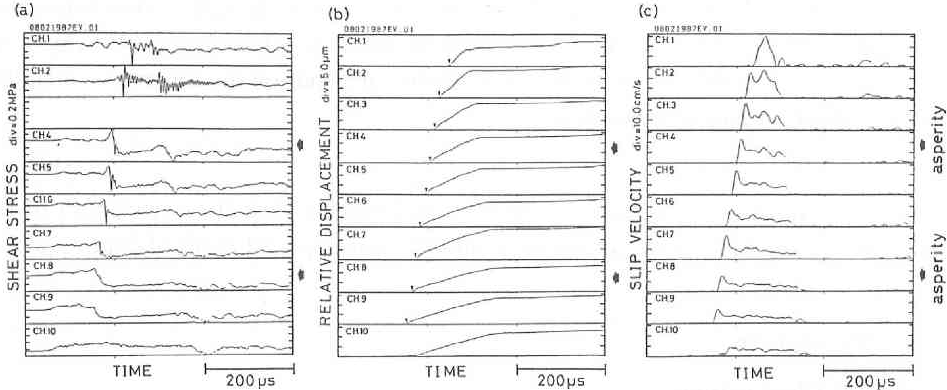
Fig. 6 The observed records of (a) shear stress, (b) relative displacement, and (c)
slip velocity for a stick-slip event at an average normal stress of 7.5 MPa.   The
onset times of rupture are indicated by solid triangles in (b).

Figs. 5(b) and 6(b).

Rigorously speaking, the rupture velocity obtained in our experiments should be
regarded as the apparent rupture velocity, because it was measured along the fault on a
free surface of the sample in spite that the rupture propagation direction (the direction
normal to the rupture front) is not always parallel to the fault strike.   When a rupture
propagates radially from a point deep in the fault plane, for example, the rupture
propagation direction and the fault strike make a significantly high angle to give an
overestimation for the rupture velocity.   However, the fault width of our sample is 10
cm and considerably small compared with the fault length of 40 cm.   Our rupture
velocity is therefore considered a good approximation to the true rupture velocity,
except for that obtained in the region of rupture nucleation.

We adopted the first peak of slip velocity time function as the maximum slip velocity
$\dot{u}_{max}$, since we are concerned particularly with the dynamic behavior of shear crack tip
in the local breakdown process.   In the case of uniform faults, the slip velocity $\dot{u}$ usually
attains its peak value just after the onset time of sudden slip.   In the present case of
nonuniform faults, however, $\dot{u}$ sometimes reached its peak value at a time considerably
later than the onset time, as seen, for instance, in CH. 6 in Fig. 5(c).   Almost all the cases
of the delayed peak in slip velocity were observed in concave areas under the average
normal stress of a considerably small value.   This complicated behavior of slip velocity
function, which is characteristic of nonuniform faults, may be interpreted as follows.   In
terms of the dislocation theory, the slip velocity is proportional to the flux of dislocation
lines per unit time, and the shear stress at the crack tip also depends on the dislocation
density near the crack tip in the cracked region.   A weak region can be broken by weak
stress concentration due to a low density of dislocation lines.   In order to break a strong
region, a high stress at the crack tip should be produced by a dislocation pile-up.   The
slip velocities at points inside the cracked region, not necessarily near the crack tip, may
depend on the motion of the crack tip ahead of the points.   When the crack tip is

decelerated, the slip velocities at the points in the cracked region may be lowered. When a strong area is broken at the crack tip, the slip at the points in the cracked regions is forced to increase rapidly to increase the slip velocity significantly. Shortly after the crack tip breaks a strong area, the local slip velocity in a weak and cracked region may thus attain a value larger than the peak value already attained during the breakdown of the weak region. It is understood from this that the first peak in the slip velocity time function should be taken as the value relating to the breakdown stress drop $\Delta\tau_b$ at the point concerned. Further, the high–frequency wave radiation from faulting may be caused by the complex behavior of slip velocity owing to the nonuniformity of sliding surfaces. It is noted that Ohnaka *et al.* (1986) have suggested that a multiple pulse in slip velocity time function corresponds to the breakdown of asperities on the fault.

Fig. 7 illustrates the space–time views of rupture propagation together with the spatial distributions in values of $\Delta\tau_b$, $\dot{u}_{max}$, and V_R obtained for events at average normal stresses of 2.5, 5.0, and 7.5 MPa. Figs. 7(a) and (c) correspond to the events shown in Figs. 5 and 6, respectively. These figures reveal that the rupture propagation was accelerated in the concave areas and decelerated in the convex areas of the sliding surfaces. The high strength areas resulting from local high normal stresses seem to behave as obstacles for the rupture propagation. The local value of V_R sometimes exceeds the S–wave velocity and reaches a value nearly equal to the P–wave velocity as seen in Fig. 7(a). This is observed in concave areas when the average normal stress is low and, consequently, the strength of the areas is considerably low. The rupture velocity in other areas is almost equal to or less than the S–wave velocity. The local values of $\Delta\tau_b$ and $\dot{u}_{max}$ were found to be larger in the convex areas than those in the concave areas. This indicates clearly that they depend on the local normal stress, as
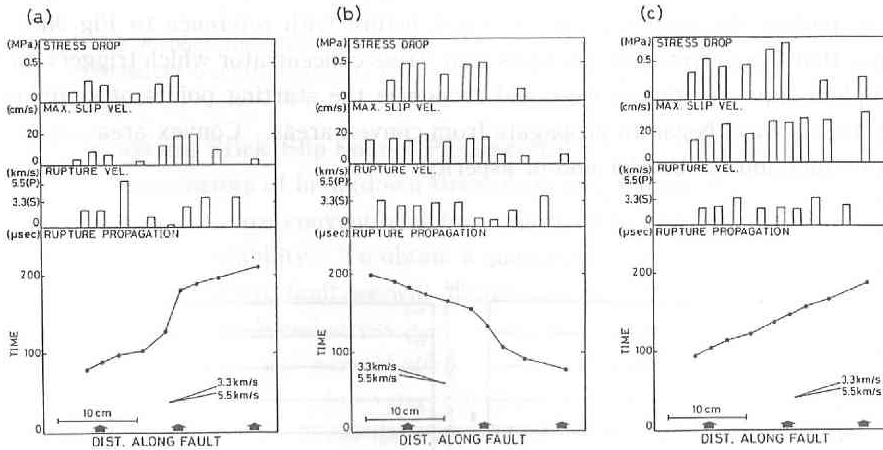

Fig. 7 The spatial distributions of breakdown stress drop, maximum slip velocity, rupture velocity, and rupture time obtained for stick-slip events at average normal stresses of (a) 2.5 MPa, (b) 5.0 MPa, and (c) 7.5 MPa. The arrows in the figures indicate approximately the center points of asperities. The events of (a) and (c) are the same ones that shown in Fig. 5 and in Fig. 6, respectively.

expected previously. It is seen also from the figures that the irregularity in rupture propagation as well as the nonuniformities in distributions of stress drop and slip velocity become weaker as the average normal stress increases, which will be discussed later.

4.2 Initiation and Termination of Rupture

A rupture stops propagating where the available strain energy is insufficient to break the cohesion between the two fault surfaces. In the case of a uniform field where the stored strain energy and the fracture energy are uniformly distributed over the medium, the rupture once breaking out would never stop. This suggests that some kinds of nonuniformity on a fault should be related to the mechanism of rupture arrest.

Fig. 8 displays an example of the shear stress and relative displacement observed for a rupture arrest event. The space–time view of the rupture propagation for this event is shown in Fig. 9(a). The rupture with an apparent velocity of about 1 km/s came to a halt at a convex area. Let us call the slip that breaks only a part of the fault surface a partial slip, hereafter. After a time interval of 550 μs the complete slip that would extend over the entire fault surface started from almost the same point where the preceding partial slip had stopped. This time interval is very long for a stick–slip event, because the S–wave travel time between two neighboring sensors, where their mutual distance is about 2 cm, is about 6 μs. The rupture was thus considered to stop propagating at the convex region. Partial slip events were observed only at the average normal stress of 2.5 MPa.

The strength at a point of the fault can be represented by the apparent fracture energy G. The value of G at each sensor position is obtained from a slip–weakening curve like Fig. 3. It is found from the G values in Fig. 9(b) that the rupture was arrested by the high resistivity of a high apparent fracture energy.

An event of complete slip started to propagate at the point where the preceding event of partial slip had stopped, as stated before with reference to Fig. 9(a). This indicates that the convex area also acts as a stress concentrator which triggers an event of complete slip. As far as we could recognize the starting points of complete slip events, they always began to propagate from convex areas. Convex areas on the fault have two functions of barrier and of asperity.
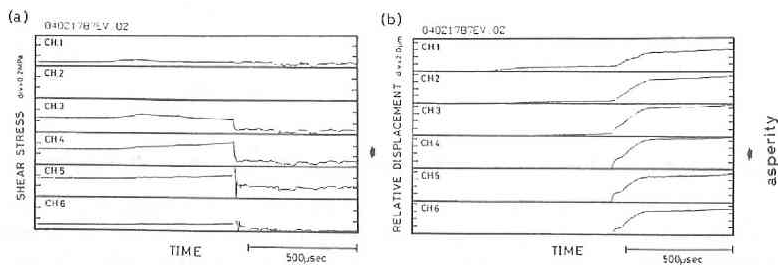

Fig. 8   The observed records of (a) shear stress, (b) relative displacement obtained for a stick–slip event in which the rupture stopped propagating at an asperity.
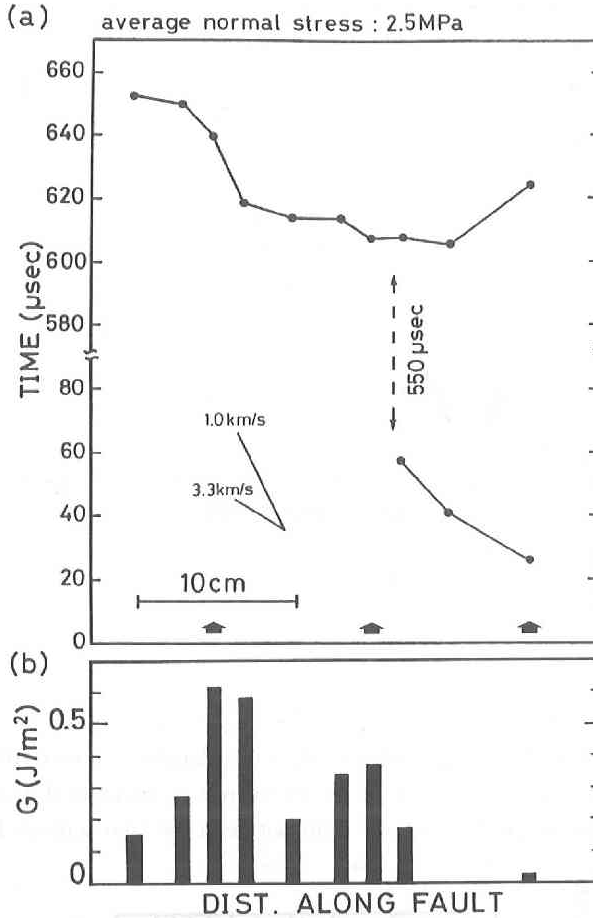
Fig. 9 (a) A space–time view of rupture propagation, and (b) the spatial distribution
of apparent fracture energy G for the same event that shown in Fig. 8.

4.3 Relations among Stick–Slip Source Parameters

The source parameters of breakdown stress drop $\Delta\tau_b$, maximum slip velocity $\dot{u}_{max}$, and rupture velocity V_R are conventional but important to characterize the dynamic behavior of the shear instability.   To obtain a quantitative understanding for the shear instability on the nonuniform fault we will discuss here the relations among these local parameters and the local normal stress σ_n.

a) *Breakdown stress drop and normal stress*

The local values of the breakdown stress drop $\Delta\tau_b$ are plotted in Fig. 10 as a function of the local normal stress σ_n.   These data were obtained for average normal stresses of 2.5, 5.0, 7.5, 10.0, 12.5 MPa from the strain sensors located at channels 2, 4, 6, and 9 in Fig. 4.   The data at different locations are distinguished by different symbols in Fig. 10. Looking at the data all together, we can observe the general tendency that $\Delta\tau_b$ increases with an increase in σ_n, though the data show a large scatter.   If we look at the data of
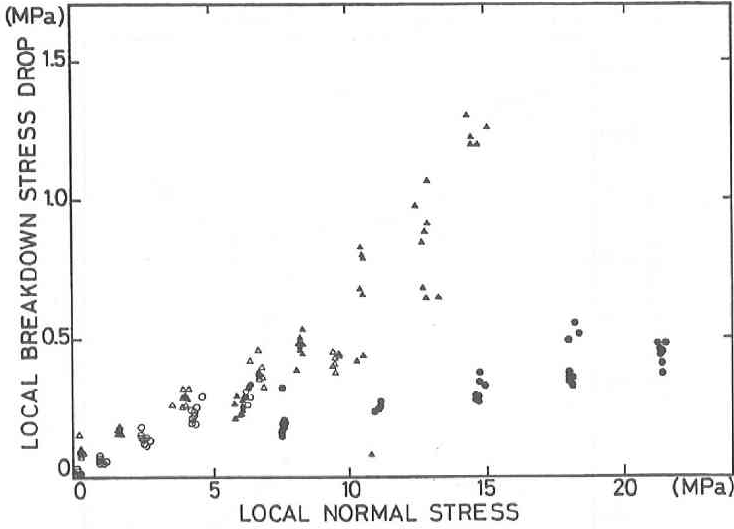
Fig. 10   The local breakdown stress drop versus the local normal stress.
Symbols distinguish observation points; open circles and triangles stand for CH.
2 and CH. 6 at concave regions, solid circles and triangles for CH. 4 and CH. 9 at
convex regions.

the same symbol separately, they lie approximately on a straight line.   The scattering
of the data is greatly reduced but still remains considerable.   The dynamic shear stress
for $\Delta\tau_b$ and the static normal stress for σ_n could not be measured exactly at the same
point.   However, the distance of about 1 cm between the two sensors for $\Delta\tau_b$ and σ_n is
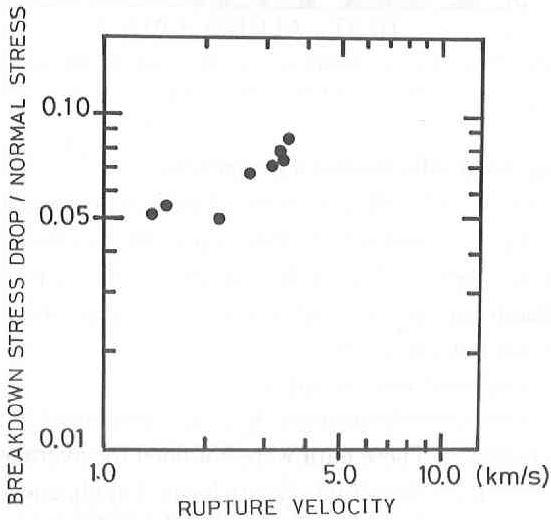

Fig. 11   The breakdown stress drop divided by local normal stress versus the rupture
velocity.   The data are obtained by CH. 9 at an average normal stress of 10.0
MPa.

much less than about 10 cm of the wavelength of waviness, suggesting that the errors arising from the small difference in sensor position cannot significantly account for the data scatter stated above.

We therefore consider that the data scatter in Fig. 10 is physically significant and that the fault strength, which is in proportion to the $\Delta\tau_b$ according to the fracture energy criterion, depends not only on the local normal stress but also on some other physical quantities. The rupture velocity may be taken as a parameter to describe the rapidity of breakdown process. In Fig. 11 we plotted against V_R the $\Delta\tau_b/\sigma_n$ data obtained at the position of CH. 9 under an average normal stress of 10.0 MPa. The relation between $\Delta\tau_b$ and σ_n is found to depend on the rupture velocity. It is noted, however, that if we plot all the data disregarding the difference in sensor position and the difference in average normal stress, we do not find such a clear dependence as seen in Fig. 11. This may be due partly to the poor accuracy in our measurement. This seems to suggest, however, that the quantity of $\Delta\tau_b/\sigma_n$ depends not only on the rupture velocity but also
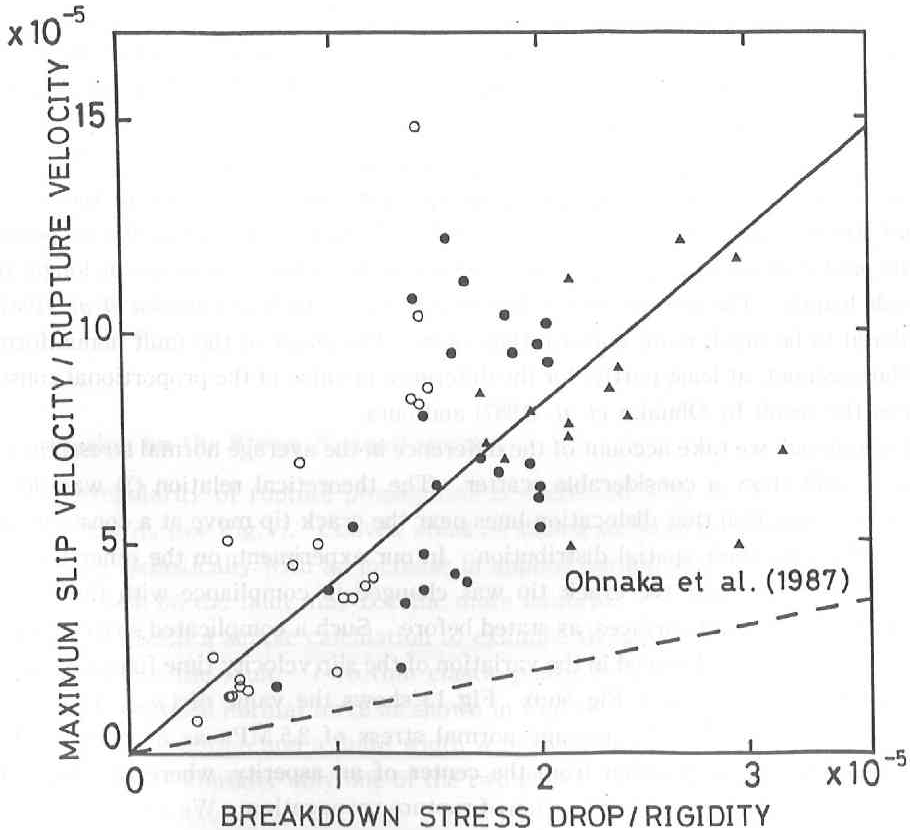

Fig. 12   The maximum slip velocity divided by rupture velocity versus the breakdown stress drop divided by rigidity. Open circles stand for the data obtained at average normal stress $\bar{\sigma}_n = 2.5$ MPa, solid circles for the data at $\bar{\sigma}_n = 5.0$ MPa, and solid triangles for the data at $\bar{\sigma}_n = 7.5$ MPa.

on some other quantity related to the time–dependent property of the fault strength.

b)   *The maximum slip velocity*

Based on the slip–weakening model, Ida (1973) derived the maximum slip velocity as

$$\dot{u}_{\max} \sim (\Delta \tau_b / \mu) \cdot V_R, \tag{3}$$

where μ is the rigidity.   Fig. 12 shows our experimental data of $\dot{u}_{\max}/V_R$ with respect to $\Delta \tau_b / \mu$.   In the figure the data obtained in the nucleation zone were excluded because of the large uncertainty in estimating the true rupture velocity as discussed before.   We also excluded the data calculated from the values of V_R smaller than 1 km/s.   The reason is that the rupture with a low V_R generally propagates rather unstationarily while we have to regard the average value between two sensor points as the value of V_R at the point concerned.   Fig. 12 indicates approximately a proportional relation between $\Delta \tau_b / \mu$ and $\dot{u}_{\max}/V_R$ as predicted by (3).   Although there exists a large scatter, the proportional constant is determined as 4.1 by a least squares method for all the data in the figure.   Ohnaka *et al*. (1987) obtained a proportional relation between these quantities from the experiment performed with the same apparatus that we used.   The proportional constant in their result is nearly equal to unity and significantly smaller than ours.

The constant may possibly be affected by the nonuniformity of the fault.   The degree of nonuniformity in stress distribution is decreased with an increase in applied normal stress, as will be seen in the next section.   The proportional constants of $\dot{u}_{\max}/V_R$ to $\Delta \tau_b / \mu$ for the data obtained at average normal stresses of 2.5, 5.0, 7.5 MPa are 5.6, 4.3, 3.5, respectively.   The value seems to decrease with an increase in the average normal stress.   Ohnaka *et al*. (1987) prepared their sliding surfaces as flat as possible, and the predominant wavelength of their unintentional surface waviness was longer than the fault length.   The normal stress distribution on the fault of Ohnaka *et al*. (1987) is considered to be much more uniform than ours.   The effect of the fault nonuniformity may thus account, at least partly, for the difference in value of the proportional constant between the result by Ohnaka *et al*. (1987) and ours.

Even though we take account of the difference in the average normal stress, the data in Fig. 12 still show a considerable scatter.   The theoretical relation (3) was derived under the assumption that dislocation lines near the crack tip move at a constant speed without changing their spatial distribution.   In our experiment, on the other hand, the dislocation density near the crack tip was changed in compliance with the strength distribution of the fault surfaces, as stated before.   Such a complicated spatial distribution of dislocations is observed in the variation of the slip velocity time function with the distance along the fault (see Fig. 5(c)).   Fig. 13 shows the value of $(\dot{u}_{\max}/V_R) \cdot (\mu / \Delta \tau_b)$ obtained from events at the average normal stress of 2.5 MPa as a function of the distance of the sensor position from the center of an asperity, where the distance is measured along the fault in the direction of rupture propagation.   We see from the figure that the values of $(\dot{u}_{\max}/V_R) \cdot (\mu / \Delta \tau_b)$ are not constant and larger at points near and beyond the asperity.   This implies that the value becomes larger when the asperity is broken.
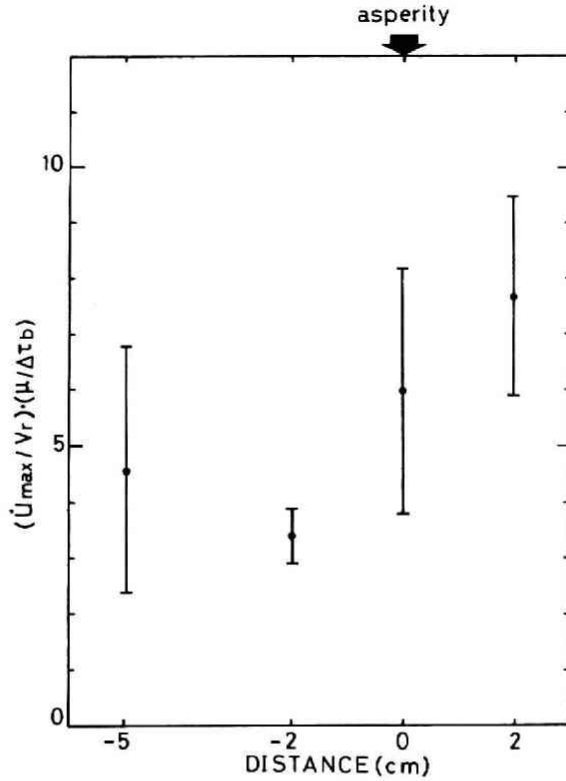
asperity

Fig. 13 The spatial distribution of $(\dot{u}_{max}/V_R)\cdot(\mu/\Delta\tau_b)$ with error bar as a function of distance along the fault. The data are obtained for stick–slip events at $\sigma = 2.5$ MPa. The direction of rupture propagation is taken as the positive direction of the abscissa.

5. Discussion on the Stress Nonuniformity

The irregularity of rupture propagation is decreased with an increase in average normal stress $\bar{\sigma}_n$ (see Fig. 7). Convex areas on sliding surfaces are deformed elastically and perhaps inelastically with an increase in applied normal stress so that the distribution of strength on the fault may become more uniform.

Let us perform a simple calculation to examine theoretically the nonuniformity of normal stress on the fault. Two thin elastic plates in a state of plane stress are in contact by an applied normal force as shown in Fig. 14, where each plate has an infinite length in the x-direction and a finite width h in the y-direction. In the mathematical modeling, we may consider only one of the two plates, say the lower plate in the figure. When the wavy boundary of the plate is free from stresses, its shape is assumed to be expressed by a sine curve as
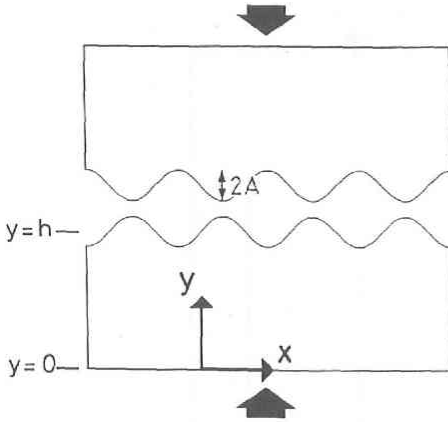
$$y = A\sin(2\pi x/L) + h. \tag{4}$$

Fig. 14 The model and the coordinates used in theoretical calculation for the normal stress distribution.

Considering our sample configuration, the values of the constants in (4) can be taken as $L=10$ cm, $h=20$ cm, and $A=5$ μm. According to the theory of elasticity (e.g. Timoshenko and Goodier, 1970), the stress function $\phi(x, y)$ should satisfy the equation

$$\nabla^4 \phi(x, y) = 0. \tag{5}$$

Next, we must specify the boundary conditions. It is reasonable to assume that the stress component of τ_{xy} is zero at the two boundaries, and that the displacement v in the y-component is fixed at $y=0$. When the applied normal force is sufficiently large, the two plates are in contact entirely and the original wavy surfaces should become flat. Since the amplitude of the surface waviness can be regarded as being infinitesimally small, the boundary conditions at the wavy surface are replaced by those at $y=h$. The boundary conditions are thus given by

$$\tau_{xy}(x, h) = \tau_{xy}(x, 0) = 0, \tag{6a}$$
$$v(x, 0) = 0, \tag{6b}$$
$$v(x, h) = -A \sin(2\pi x/L) - B, \tag{6c}$$

where B is a constant.

To satisfy (6c) the stress function $\phi(x, y)$ should have the form

$$\phi(x, y) = \sin(2\pi x/L) \cdot f(y) + C_0 x^2, \tag{7}$$

where C_0 and $f(y)$ are an unknown constant and an unknown function, and $C_0 x^2$ is related to a uniform stress field. Substituting (7) into (5), we have a differential equation for $f(y)$. Its general solution is given by Timoshenko and Goodier (1970) as

$$f(y) = C_1 \cosh(2\pi y/L) + C_2 \sinh(2\pi y/L) + C_3 y \cosh(2\pi y/L) + C_4 y \sinh(2\pi y/L), \tag{8}$$

where C_1, C_2, C_3, C_4 are constants. Using the static elastic constants of Higashiyama granite, we determine the constants C_0, C_1, C_2, C_3, C_4 from (6) with given values of B. When B is equal to A, the wavy surface just become flat, as understood from (4) and (6c). The average value of the normal stress at $y=h$ is calculated to be 8.8 MPa in this case.
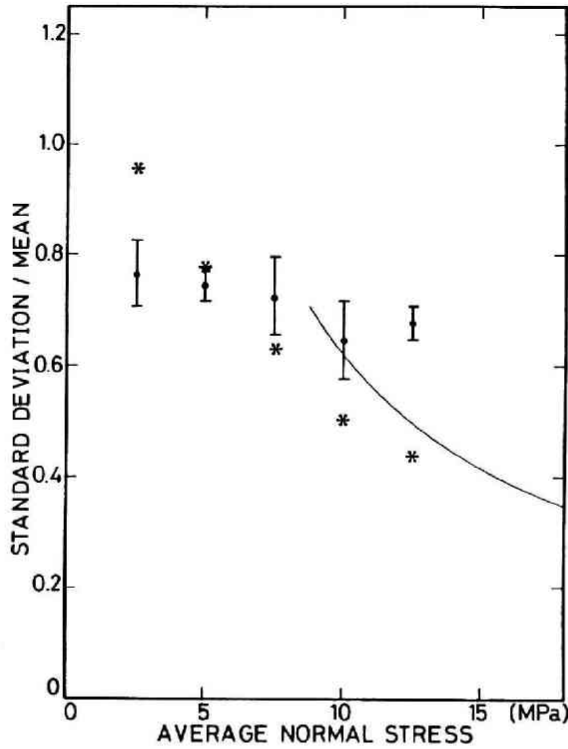
Fig. 15 Standard deviations of local normal stress and breakdown stress drop divided by their respective mean values plotted against average normal stress. The asterisks stand for the observed local normal stress, and the solid circles with error bar for the observed breakdown stress drop. The solid line indicates the theoretical local normal stress.

In other words, the two plates are not entirely in contact until the applied normal stress becomes 8.8 MPa.

The standard deviation divided by its mean value, s/m, is used for a measure of nonuniformity in stress distribution. Fig. 15 shows the theoretical s/m curve of the local normal stress computed for $B \geq A$ (or average normal stresses larger than 8.8 MPa) in comparison with the s/m values of the observed local normal stress (asterisks) and the observed breakdown stress drop (dots with error bar). Here, the observed local normal stresses were measured at two points in convex areas and at two points in concave areas in our experiment. The observed breakdown stress drops were measured at 13 points. All the three quantities in the figure are found to decrease as the average normal stress increases.

Although the decay patterns of the nonuniformities s/m for the theoretical normal stress and for the observed one are similar to each other, there is some difference in the absolute value between them. This difference may arise from our assumption of perfect linear elasticity, for example, in the theoretical calculation. In fact the observed normal

stresses at concave areas did not seem to be zero even at the average normal stress of 2.5 MPa.

The figure shows that the nonuniformity of the observed breakdown stress drop is decreased much more gently with an increase in the average normal stress than that of the local normal stress. It is worth while noting that the nonuniformity of the breakdown stress drop may remain significant even when the local normal stress distribution on the fault becomes quite uniform.

6. Summary and Conclusions

The general features of shear instability on a nonuniform strength fault were examined using a granite sample with wavy fault surfaces. When a normal force is externally applied to the fault surfaces, the convex area of the wavy fault becomes a relatively high strength area due to high local normal stresses. The rupture is accelerated in concave regions and decelerated in convex regions, and the breakdown stress drop and the maximum slip velocity in convex regions are higher than those in concave regions. It is found that the propagation of rupture developed in a concave region is sometimes arrested in a convex region, where the convex region acts as a barrier having a high fracture energy. The complete slip that extends over the entire fault is found to start propagating rapidly when the barrier is broken, where the convex region is regarded as an asperity. This implies that the initiation and termination processes of earthquake faulting are governed mainly by the deformation behavior of strong regions on faults.

Our experimental data show that the breakdown stress drop $\varDelta\tau_b$ is roughly proportional to the local normal stress σ_n. This agrees with the results of previous experimental studies. Further, a proportional relation is found between $\dot{u}_{\max}/V_R$ and $\varDelta\tau_b/\mu$ to a first approximation, where $\dot{u}_{\max}$ and V_R are the local values of the maximum slip velocity and the rupture velocity, and μ is the rigidity. This is consistent not only with the theoretical result by, for instance, Ida (1973) but also with the experimental one by Ohnaka et al. (1987). Rigorously speaking, however, either $\varDelta\tau_b/\sigma_n$ or $(\dot{u}_{\max}/V_R)\cdot(\mu/\varDelta\tau_b)$ is not constant. In fact, $\varDelta\tau_b/\sigma_n$ is found to depend on V_R. The value of $(\dot{u}_{\max}/V_R)\cdot(\mu/\varDelta\tau_b)$ at a point seems to be influenced by the strength distribution in the surrounding area on the fault. In order to establish properly the relationships among these source parameters, it seems necessary to take into consideration the effect of the time (or strain rate) dependent property of fault strength.

The arrest of rupture propagation at an asperity was observed at a low average normal stress. The irregularity in rupture propagation is generally reduced as the average normal stress increases. This is because the spatial distribution of local normal stress becomes more uniform as asperities are deformed to be flatter. Interestingly, however, the nonuniformity of the breakdown stress drop (or the shear strength of the fault) remains significant in contrast to a significant decrease in nonuniformity of the local normal stress with an increase in the average normal stress.

Generally speaking, the geological faults that appear on the earth's surface are not

simply linear but complicated and irregular. It is natural to expect that this complexity extends deep in earthquake fault. Our experimental results suggest that the irregular motion in earthquake faulting depends strongly on the nonuniform distribution of normal stress on the fault due to the irregular surface topography.

References

Archuleta, R.J. and J.N. Brune, 1975 : Surface strong motion associated with a stick-slip event in a foam rubber model of earthquakes, *Bull. Seism. Soc. Am.*, **65**, 1059-1071.

Brace, W.F. and J.D. Byerlee, 1966 : Stick-slip as a mechanism for earthquakes, *Science*, **153**, 990-992.

Brune, J.N., 1970 : Tectonic stress and the spectra of seismic shear waves from earthquakes, *J. Geophys. Res.*, **75**, 4997-5009.

Brune. J.N., 1973 : Earthquake modeling by stick-slip along precut surfaces in stressed foam rubber, *Bull. Seism. Soc. Am.*, **63**, 2105-2119.

Das, S. and K. Aki, 1977 : Fault plane with barriers : a versatile earthquake model, *J. Geophys. Res.*, **82**, 5658-5670.

Ida, Y., 1972 : Cohesive force across the tip of a longitudinal-shear crack and Griffith's specific surface energy, *J. Geophys. Res.*, **77**, 3796-3805.

Ida, Y., 1973 : The maximum acceleration of seismic ground motion, *Bull. Seism. Soc. Am.*, **63**, 959-968.

Israel, M. and A. Nur, 1979 : A complete solution of a one dimensional propagating fault with nonuniform stress and strength, *J. Geophys. Res.*, **84**, 2223-2234.

Johnson, T.L. and C.H. Scholz, 1976 : Dynamic properties of stick-slip friction of rock, *J. Geophys. Res.*, **81**, 881-888.

Johnson, T.L., F.T. Wu, and C.H. Scholz, 1973 : Source parameters for stick-slip and for earthquakes, *Science*, **179**, 278-280.

Kuwahara, Y., 1985 : An experimental study on dynamic sliding process during stick-slip and its implication to earthquake faulting, Ph. D. Thesis, Tôhoku University, 130 pp.

Kuwahara, Y., M. Ohnaka, K. Yamamoto, N. Kato, and T. Hirasawa, 1986 : Accelerating process of rupture propagation during stick-slip failure instability, *Ann. Meet. Seism. Soc. Japan Abstr.*, **2**, 233 (in Japanese).

Mikumo, T. and T. Miyatake, 1978 : Dynamical rupture process on a three-dimensional fault with non-uniform frictions and near-field seismic waves, *Geophys. J.R. astr. Soc.*, **54**, 417-438.

Ohnaka, M., K. Yamamoto, Y. Kuwahara, and T. Hirasawa, 1983 : Dynamic processes during slip of stick-slip as an earthquake fault model, *Zisin*, **36**, 53-62 (in Japanese).

Ohnaka, M., Y. Kuwahara, K. Yamamoto, and T. Hirasawa, 1986 : Dynamic breakdown processes and the generating mechanism for high-frequency elastic radiation during stick-slip instabilities, in *Earthquake Source Mechanics* (edited by S. Das, J. Boatwright, and C.H. Scholz), *A.G.U. Maurice Ewing Ser.*, **6**, 13-24.

Ohnaka, M., Y. Kuwahara, and K. Yamamoto, 1987 : Constitutive relations between dynamic physical parameters near a tip of the propagating slip zone during stick-slip shear failure, *Tectonophysics*, **144**, 109-125.

Okubo, P.G. and J.H. Dieterich, 1981 : Fracture energy of stick-slip events in a large scale biaxial experiment, *Geophys. Res. Lett.*, 8, 887-890.

Okubo, P.G. and J.H. Dieterich, 1984 : Effects of physical fault properties on frictional instabilities produced on simulated faults, *J. Geophys. Res.*, 89, 5817-5827.

Palmer, A.C. and J.R. Rice, 1973 : The growth of slip surfaces in the progressive failure of over-consolidated clay, *Proc. Roy. Soc. Lond.*, A332, 527-548.

Sato, T. and T. Hirasawa, 1973 : Body wave spectra from propagating shear cracks, *J. Phys. Earth*, 21, 415-431.

Timoshenko, S.P. and J.N. Goodier, 1970 : *Theory of Elasticity*, Third ed., McGraw-Hill, New York, 567 pp.

Wu, F.T., K.C. Thomson, and H. Kuenzler, 1972 : Stick-slip propagation velocity and seismic source mechanism, *Bull. Seism. Soc. Am.*, 62, 1621-1628.